



Published in final edited form as:

Bioorg Med Chem. 2012 January 1; 20(1): 47–57. doi:10.1016/j.bmc.2011.11.032.

Bisubstrate analogue inhibitors of 6-hydroxymethyl-7,8-dihydropterin pyrophosphokinase: New design with improved properties

Genbin Shi^a, Gary Shaw^a, Yu-He Liang^a, Priadarsini Subburaman^a, Yue Li^b, Yan Wu^b, Honggao Yan^b, and Xinhua Ji^{a,*}

^aMacromolecular Crystallography Laboratory, National Cancer Institute, Frederick, MD 21702, USA

^bDepartment of Biochemistry and Molecular Biology, Michigan State University, East Lansing, MI 48824, USA

Abstract

6-Hydroxymethyl-7,8-dihydropterin pyrophosphokinase (HPPK), a key enzyme in the folate biosynthetic pathway, catalyzes the pyrophosphoryl transfer from ATP to 6-hydroxymethyl-7,8-dihydropterin. The enzyme is essential for microorganisms, is absent from humans, and is not the target for any existing antibiotics. Therefore, HPPK is an attractive target for developing novel antimicrobial agents. Previously, we characterized the reaction trajectory of HPPK-catalyzed pyrophosphoryl transfer and synthesized a series of bisubstrate analog inhibitors of the enzyme by linking 6-hydroxymethylpterin to adenosine through 2, 3, or 4 phosphate groups. Here, we report a new generation of bisubstrate analog inhibitors. To improve protein binding and linker properties of such inhibitors, we have replaced the pterin moiety with 7,7-dimethyl-7,8-dihydropterin and the phosphate bridge with a piperidine linked thioether. We have synthesized the new inhibitors, measured their K_d and IC_{50} values, determined their crystal structures in complex with HPPK, and established their structure-activity relationship. 6-Carboxylic acid ethyl ester-7,7-dimethyl-7,8-dihydropterin, a novel intermediate that we developed recently for easy derivatization at position 6 of 7,7-dimethyl-7,8-dihydropterin, offers a much high yield for the synthesis of bisubstrate analogs than that of previously established procedure.

Keywords

Antibacterial; Bisubstrate; Folate; HPPK; Pterin

*Corresponding author. Tel: +1 (301) 846-5035; Fax: +1 (301) 846-6073. jix@mail.nih.gov (X. Ji).

The coordinates and structure factors have been deposited in the PDB under entry codes 3UD5 (HPPK•17), 3UDE (HPPK•18), and 3UDV (HPPK•19).

Supplementary data

Supplementary data (the ¹H and ¹³C spectra of compounds 7, 8, 16, 17, and 19) associated with this article can be found, in the online version, at...

Publisher's Disclaimer: This is a PDF file of an unedited manuscript that has been accepted for publication. As a service to our customers we are providing this early version of the manuscript. The manuscript will undergo copyediting, typesetting, and review of the resulting proof before it is published in its final citable form. Please note that during the production process errors may be discovered which could affect the content, and all legal disclaimers that apply to the journal pertain.

1. Introduction

Folate cofactors are essential for life.¹ Mammals derive folates from their diet, whereas most microorganisms must synthesize folates *de novo*.² Therefore, the folate pathway has been a promising target for developing antimicrobial agents.^{3–9} For example, inhibitors of dihydropteroate synthase and dihydrofolate reductase, two key enzymes in the pathway, are currently used in clinic as antibiotics.^{10–12} 6-Hydroxymethyl-7,8-dihydropterin pyrophosphokinase (HPPK, E.C. 2.7.6.3) is another key enzyme in the pathway. It is essential for microorganisms, is absent from mammals, and is not the target for any existing antibiotics. Therefore, the enzyme has been explored as an attractive target for developing novel antimicrobial agents.^{13–17}

HPPK catalyzes the transfer of pyrophosphate from ATP to 6-hydroxymethyl-7,8-dihydropterin (HP) (Fig. 1A).¹⁸ The reaction follows an apparently ordered kinetic mechanism with MgATP binding to the enzyme first followed by rapid addition of HP; the K_d for the binding of MgATP to HPPK is 2.6–4.5 μM , and the K_d for the binding of HP to the HPPK MgATP complex is in the sub- μM range.^{19–21} In contrast, the K_d for the binding of HP to ligand-free HPPK is in the mM range.²² The cellular ATP concentration is estimated to be ~ 3 mM.²³ Therefore, the enzyme is essentially in the MgATP-bound form, ready for the addition of HP. The products of the reaction are AMP and 6-hydroxymethyl-7,8-dihydropterin pyrophosphate (HPPP, Fig. 1A) and the release of reaction products is rate limiting.²¹ In-depth structural and mechanistic studies of the enzyme ensured that HPPK is currently the best understood pyrophosphokinase.^{24,25}

Two types of HPPK inhibitors have been developed previously.²⁴ Type 1 inhibitors are HP derivatives, including 6-hydroxymethyl-7,7-dimethyl-7,8-dihydropterin (HP-1, Fig. 1B)^{13,15} and 6-hydroxymethyl-7-methyl-7-phenethyl-7,8-dihydropterin (HP-3, Fig. 1C).¹⁶ Type 2 inhibitors are bisubstrate analogues P^1 -(6-hydroxymethylpterin)- P^2 -(5'-adenosyl)diphosphate, P^1 -(6-hydroxymethylpterin)- P^3 -(5'-adenosyl)triphosphate, P^1 -(6-hydroxymethylpterin)- P^4 -(5'-adenosyl)tetrakisphosphate (HP_nA; n=2, 3, or 4, Fig. 1D).¹⁷ However, HP-1 is degraded during prolonged incubation with HPPK,¹⁵ the phenethyl group of HP-3 disturbs the geometry of enzyme active site significantly,^{16,24} which may lead to low binding affinity, and the phosphate bridge of HP_nA carries many negative charges,¹⁷ which may lead to poor bioavailability. Although none of these compounds are considered useful inhibitors of HPPK,²⁶ they provide valuable information for further development. Here, we present improved bisubstrate analog inhibitors of HPPK, which we have designed on the basis of useful features of aforementioned inhibitors.

2. Results and discussion

2.1. Design

In the catalytic complex of HPPK,^{16,27,28} pterin is recognized by HPPK via five hydrogen bonds (Fig. 2A); so is adenosine (Fig. 2B). The phosphate bridge, however, is bound optimally only when the phosphoryl transfer reaction is about to occur. One effective approach to enhance the specificity and potency in enzyme inhibition is to design multisubstrate analogs.^{29,30} Among the three bisubstrate analogs we have previously developed, HP₄A is the most potent inhibitor of HPPK ($K_d = 0.47$ and $\text{IC}_{50} = 0.44$ μM).¹⁷ The overall structure of the protein in the HPPK•MgHP₄A complex (PDB entry 1EX8)¹⁷ is similar to that observed in the HPPK•MgAMPCPP•HP complex (PDB entry 1Q0N)²⁷ and the pterin and adenosine moieties of HP₄A superimpose well with their counterparts in the ternary complex.¹⁷ The pterin-protein and adenosine-protein interactions are conserved in the two structures with one exception. In HPPK•MgAMPCPP•HP, N8 of HP is hydrogen bonded to the backbone carbonyl oxygen of L45 (Fig. 2A). In HPPK•MgHP₄A, however,

this hydrogen bond does not exist because the pterin moiety of HP₄A is oxidized (Fig. 1D) and thus N8 cannot serve as a hydrogen bond donor. Under normal conditions, HP is readily oxidized at the 7 and 8 positions, which can be effectively prevented by the introduction of two methyl groups at position 7 as those in HP-1 (Fig. 1B). As expected, the hydrogen bond between N8 of the inhibitor and carbonyl oxygen of L45 has been observed in the crystal structure of HPPK in complex with HP-1 (PDB entry 1CBK).¹⁵ Furthermore, in the HPPK•HP-1 structure, the 7,7-dimethyl group of HP-1 interacts favorably with the W89 side chain of HPPK.

As aforementioned, the phosphate bridge of HP₄A carries several negative charges that may lead to poor bioavailability. Besides, the intact ATP moiety as part of the inhibitor may result in unwanted interaction with other kinases. At this stage of the development, we have modified the HP₄A structure in two respects. First, we have replaced the phosphate bridge with a piperidine linkage (Fig. 2C). Second, we have introduced two methyl groups at position 7 of the pterin moiety (Fig. 2D). Using the piperidine, which is seen in other drug molecules, we can eliminate the negative charges carried by the linkage and also diminish unwanted binding of the inhibitor by other kinases. Introducing the 7,7-dimethyl group, we can effectively prevent the hydrogen bond donor N8 from being oxidized and thereby promote the formation of the hydrogen bond between N8 and carbonyl oxygen of L45. The resulting structures fit nicely in the active center of HPPK (not shown).

2.2. Synthesis

Compounds **7**, **8**, and **16–19** are new, whereas the rest are either known or commercially available. Using commercially available 2',3'-isopropylideneadenosine (**1**, Scheme 1), we followed the Sakami method³¹ to synthesize 2',3'-O-isopropylidene-5'-O-toluene-p-sulfonyl adenosine (**2**), during which an anhydrous pyridine solution of **1** was shaken with p-toluenesulfonyl chloride. The synthetic intermediate 4-acetylsulfanyl-piperidine-1-carboxylic acid tert-butyl ester (**4**) was synthesized by using the method of Plettenburg et al.³² in which potassium thioacetate and 4-bromo-piperidine (**3**) were heated in DMF. According to a modified procedure based on an existing protocol,³³ **4** reacted with sodium methoxide to form the thiol, followed by the reaction with **2** to give 4-[6-(6-amino-purin-9-yl)-2,2-dimethyl-tetrahydro-furo[3,4-d][1,3]dioxol-4-ylmethylsulfanyl]-piperidine-1-carboxylic acid tert-butyl ester (**5**). Under the TFA/DCM condition, cleavage of the BOC protection group yielded 9-[2,2-dimethyl-6-(piperidin-4-ylsulfanylmethyl)-tetrahydro-furo[3,4-d][1,3]dioxol-4-yl]-9*H*-purin-6-ylamine (**6**) and the subsequent reaction of **6** with (2-bromo-ethyl)-carbamic acid tert-butyl ester provided the key intermediate (2-{4-[6-(6-amino-purin-9-yl)-2,2-dimethyl-tetrahydro-furo[3,4-d][1,3]dioxol-4-ylmethylsulfanyl]-piperidin-1-yl}-ethyl)-carbamic acid tert-butyl ester (**7**). The deprotection of **7** yielded 2-[1-(2-amino-ethyl)-piperidin-4-ylsulfanylmethyl]-5-(6-amino-purin-9-yl)-tetrahydro-furan-3,4-diol (**8**) that contained an amino group that would be used to link **8** to the pterin moiety.

A total of four pterin moieties were synthesized, including 6-bromomethylpterin (**11**, Scheme 2), 6-bromomethyl-7,7-dimethyl-7,8-dihydropterin (**13**, Scheme 3), 6-carbaldehyde-7,7-dimethyl-7,8-dihydropterin (**14**, Scheme 3), and 6-carboxy-7,7-dimethyl-7,8-dihydropterin (**16**, Scheme 3).

Compound **11** was synthesized as described.¹⁴ Briefly, 2,4-diamino-6-(hydroxymethyl)pteridine hydrochloride (**9**, Scheme 2) was treated with dibromotriphenylphosphorane in *N,N*-dimethylacetamide to give 6-bromomethyl-pteridine-2,4-diamine (**10**). In 48% hydrobromic acid, **10** was converted through hydrolytic deamination to **11** (Scheme 2).

The other three pterin moieties were derived from 2-amino-7,8-dihydro-6,7,7-trimethylpteridin-4(3*H*)-one (**12**, Scheme 3) synthesized by a procedure of Al-Hassan et al.¹⁴ Subsequently, **12** was converted to **13** by Stuart's method³⁴ using bromine in acetic acid solution, oxidized by SeO₂ in DMF to give **14**, or converted to **16** through 2-amino-7,7-dimethyl-4-oxo-3,4,7,8-tetrahydro-pteridine-6-carboxylic acid ethyl ester (**15**) by heating **12** with bromine in ethanol solution followed by ester bond hydrolysis in base and methanol (Scheme 3). The conditions for the conversion of **12** into **14**, and the intermediate (**15**) for the derivation of **16** from **12** are as recently described.³⁵

The final step of the synthesis is outlined in Scheme 4, resulting in three final products: 2-amino-6-[(2-{4-[5-(6-amino-purin-9-yl)-3,4-dihydroxy-tetrahydro-furan-2-ylmethylsulfanyl]-piperidin-1-yl}-ethylamino)-methyl]-3*H*-pteridin-4-one (**17**), 2-amino-6-[(2-{4-[5-(6-amino-purin-9-yl)-3,4-dihydroxy-tetrahydro-furan-2-ylmethylsulfanyl]-piperidin-1-yl}-ethylamino)-methyl]-7,7-dimethyl-7,8-dihydro-3*H*pteridin-4-one (**18**), and 2-amino-7,7-dimethyl-4-oxo-3,4,7,8-tetrahydro-pteridine-6-carboxylic acid (2-{4-[5-(6-amino-purin-9-yl)-3,4-dihydroxy-tetrahydro-furan-2-ylmethylsulfanyl]-piperidin-1-yl}-ethyl)-amide (**19**). Compound **17** was synthesized by allowing **8** and **11** to react. Compound **18** was derived from **8** and **13** in DMF solution with potassium carbonate. Compound **19** was obtained by two procedures: the procedure developed by Yoo and Li³⁶ using copper-silver catalysis and aqueous tert-butyl hydroperoxide (Method A) and the procedure developed by us³⁵ using the new intermediate **15** (Method B) with a significantly improved yield.

2.3. HPPK binding and inhibition

The K_d and IC₅₀ measurements were carried out as described.^{37,17} The K_d value is > 150 μM for **17** and 2.55 ± 0.15 μM for **19**, and the IC₅₀ value is > 100 μM for **17** and 3.16 ± 0.34 μM for **19**. Compound **18** was not stable, and therefore, its K_d and IC₅₀ were not determined. These data show that **19** has a 60-fold increased binding affinity and 30-fold increased inhibition ability over **17**.

2.4. Crystal structures of compounds **17**, **18**, and **19** each in complex with HPPK

Although **18** was not stable, it was stabilized when bound to HPPK. HPPK in complex with **17**, **18**, or **19** was crystallized (Table 1) and the crystal structures of all three complexes (HPPK•**17**, HPPK•**18**, and HPPK•**19**) were determined (Table 2). The HPPK•**17** structure (Fig. 3A) contains 1 HPPK (residues 1–158), 1 compound **17**, 1 ethylene glycol, and 106 water molecules. The HPPK•**18** structure (Fig. 3B) contains 1 HPPK (residues 1–82, 87–158), 1 compound **18**, 1 acetate ion, and 88 water molecules. The HPPK•**19** structure (Fig. 3C) contains 1 HPPK (residues 1–82, 87–158), 1 compound **19**, 1 acetate ion, and 91 water molecules. Residues 83–86 in HPPK•**18** and HPPK•**19** were not observed and presumably disordered.

2.5. Structure-activity relationship

2.5.1. Protein conformation and inhibitor binding—HPPK has three flexible loops (Loop 1, residues 8–15; Loop 2, residues 43–53; Loop 3, residues 82–92), among which Loop 3 undergoes dramatic conformational changes during catalysis.^{22,38} The catalytic trajectory of HPPK can be described by six consecutive states: ligand-free HPPK, HPPK•MgATP, HPPK•MgATP•HP, HPPK•MgAMP-PP-HP (the transition state), HPPK•AMP•HPPP, and HPPK•HPPP.^{21,39} In the HPPK•MgATP state, Loop 3 exhibits open conformation as seen in the HPPK•MgADP [Protein Data Bank (PDB) entry 1EQM] and HPPK•MgAMPPCP (PDB entry 1EQ0) structures.³⁸ Loop 3 is also open in the HPPK•AMP•HPPP state (PDB entry 1RAO).³⁹ In the HPPK•MgATP•HP state, in contrast,

Loop 3 is closed as seen in the HPPK•MgAMPCPP•HP structure (PDB entry 1Q0N).²⁷ In the HPPK•MgATP state, however, Loop 3 has been seen to have a closed conformation in the HPPK•MgAMPCPP complex (PDB entry 2F65),⁴⁰ suggesting that Loop 3 in the HPPK•MgATP state is dynamic.²⁵

The polypeptide chains in the HPPK•**17**, HPPK•**18**, and HPPK•**19** structures superimpose well except for Loop 3 (Fig. 4A). The adenosine moieties in the three inhibitors superimpose well; so do the pterin moieties. The linkers in **18** and **19** superimpose well, but the linker in **17** displays a different conformation. In HPPK•**17**, Loop 3 displays the open conformation (Fig. 5A). During HPPK catalysis, the open Loop 3 facilitates HP binding and product release. For enzyme inhibition, however, the open conformation of Loop 3 has negative impact on binding, which is in agreement with the K_d value for the binding of **17** to HPPK ($> 150 \mu\text{M}$). As aforementioned, the K_d for the binding of MgATP to HPPK is $2.6\text{--}4.5 \mu\text{M}$. Therefore, **17** is not a good inhibitor. In contrast, Loop 3 assumes the closed conformation in the HPPK•**18** and HPPK•**19** structures although residues 83–86 in the loop are disordered (Fig. 4A, 5B). During HPPK catalysis, a closed Loop 3 seals the active center for the reaction to occur. For enzyme inhibition, a closed Loop 3 enhances the affinity for the enzyme and consequently the potency of an inhibitor. Consistently, compound **19** shows a much higher binding affinity ($K_d = 2.55 \mu\text{M}$). The K_d value of **19** is comparable with that of MgATP, suggesting the compound is a good inhibitor of HPPK.

2.5.2. Protein conformation and inhibitor structure—To form the catalytic assembly of HPPK•MgATP•HP in the closed conformation, conserved residues N10 (of Loop 1) and Q50 (of Loop 2) function as the center of a hydrogen bond network with the backbone carbonyl groups of P47 and P51 of Loop 2 and with the backbone amide and/or carbonyl groups of W89, P91, and R92 of Loop 3.²⁷ This hydrogen bond network couples all three loops and helps stabilize the complex and seal the active center. The structures show that such a hydrogen bond network exists in HPPK•**18** and HPPK•**19**, but not in HPPK•**17** (Fig. 4B).

The only differences between **18** and **17** are in positions 7 and 8 of the pterin moiety (Scheme 4). In **18**, the 7,7-dimethyl group keeps the NH group at position 8 in its reduced form, allowing the formation of the hydrogen bond between N8 and the carbonyl oxygen of L45 ($\text{N8}^{\text{Pterin}}\cdots\text{O}^{\text{L45}}$). In contrast, the dimethyl group is absent from **17** and the pterin moiety is oxidized with an N instead of an NH group at position 8, rendering the formation of the $\text{N8}^{\text{Pterin}}\cdots\text{O}^{\text{L45}}$ hydrogen bond impossible.

The impact of the formation of $\text{N8}^{\text{Pterin}}\cdots\text{O}^{\text{L45}}$ is twofold. First, it is one of the five hydrogen bonds for the recognition of HP by HPPK (Fig. 2A) and therefore contributes to protein-ligand affinity. Second, by anchoring L45 it optimizes the conformation of Loop 2 and Loop-2 residues, especially Q50, favoring the formation of the hydrogen bond network that couples and stabilizes the three loops (Fig. 4B). Taken together, these structures show that the $\text{N8}^{\text{Pterin}}\cdots\text{O}^{\text{L45}}$ hydrogen bond facilitates the formation of the hydrogen bond network that couples the three loops as seen in the closed HPPK•MgATP•HP state. A good inhibitor, such as **19**, should not impair the coupling of these loops.

As aforementioned, the 7,7-dimethyl group in HPPK•HP-1 interacts with the side chain of W89.¹⁵ This hydrophobic interaction is also observed in HPPK•**19**, whereas it is not possible in HPPK•**17** (Fig. 4B). In addition to the 7,7-dimethyl group, **19** has a new carbonyl group next to the pterin moiety (Scheme 4). It does not, however, affect the conformation of the protein.

2.5.3. Inhibitor structure and stability—Compound **17** is stable, but **18** tends to degrade when not in complex with HPPK. The only difference between **17** and **18** is that the pterin moiety in **17** is oxidized, but it is reduced in **18**. Compound **19** is stable. The only difference between **18** and **19** is that the methylene group ($-\text{CH}_2-$) at position 13 in **18** becomes a carbonyl group ($-\text{CO}-$) in **19** (Scheme 4).

2.5.4. Partial disorder of Loop 3 and protein-linker interaction—Although **19** is a good inhibitor of HPPK, Loop 3 residues 83–86 in HPPK•**19** are disordered (Fig. 4A). Furthermore, all three loops in HPPK•**19** display noticeable differences when compared with those in the HPPK•MgAMPCPP•HP structure (Fig. 5B). Such disorder and differences indicate that the protein-linker interactions are not optimized in HPPK•**19** although the three loops of the enzyme are coupled and the complex assumes the overall closed conformation. We need to further modify the linker between the pterin and adenosine moieties of **19**, which we believe will lead to higher binding affinity. In the HPPK•MgATP•HP state, the phosphate bridge is recognized by conserved HPPK side chains R82, R92, H115, and R121 (Fig. 2B). Therefore, hydrogen bond acceptors should be introduced into the linker.

3. Conclusions

We report a new generation of bisubstrate analog inhibitors of HPPK, compounds **17**, **18**, and **19** (Scheme 4). In complex with HPPK, these compounds share a common adenosine-protein interaction pattern, but their pterin moieties interact with the protein differently. In HPPK•**18** and HPPK•**19**, the $\text{N}8^{\text{Pterin}}\dots\text{O}^{\text{L45}}$ hydrogen bond is formed between pterin atom N8 (donor) of the inhibitor and carbonyl oxygen (acceptor) of L45, whereas in HPPK•**17**, the formation of this hydrogen bond is impossible. The structures show that the formation of $\text{N}8^{\text{Pterin}}\dots\text{O}^{\text{L45}}$ is sufficient to facilitate the coupling of the three loops of HPPK in the manner as seen in the HPPK•MgAMPCPP•HP complex.²⁷ Without the $\text{N}8^{\text{Pterin}}\dots\text{O}^{\text{L45}}$ interaction, the HPPK•**17** complex exhibits the open conformation without the coupling of the three loops and the binding affinity of **17** is low ($K_d > 150 \mu\text{M}$). With the formation of $\text{N}8^{\text{Pterin}}\dots\text{O}^{\text{L45}}$, in contrast, the HPPK•**19** complex displays the closed conformation due to the coupling of the three loops and the affinity of **19** is ~60-fold higher. Introducing the 7,7-dimethyl groups into **17** results in **18**, which triggers the transition of the open conformation (in HPPK•**17**) into the closed form (in HPPK•**18**). Nevertheless, **18** is not stable when it is not in complex with the enzyme. It is the replacement of the methylene group in $\text{N}=\text{CH}-\text{CH}_2-\text{NH}$ of **18** with the carbonyl group in $\text{N}=\text{CH}-\text{CO}-\text{NH}$ of **19** that improves the chemical stability (Scheme 4).

With and without the $\text{N}8^{\text{Pterin}}\dots\text{O}^{\text{L45}}$ interaction, the binding mode of the linker is also different (Fig. 4A), underscoring the importance of an ordered and closed Loop 3 for optimized protein-inhibitor interaction. For pyrophosphoryl transfer, the phosphate groups of ATP interact with four conserved side chains, R82, R92, H115, and R121 (Fig. 2B). None of these side chains interacts favorably with the linker of any of the three compounds (**17**, **18**, and **19**). Further development of bisubstrate analog inhibitors should allow favorable interactions between the linker of inhibitor and the four positively charged side chains of HPPK. Residues R82 and R92 define the boundary of Loop 3. Favored interactions between these two side chains and inhibitor should lead to a completely ordered and closed Loop 3 in the protein-inhibitor complex.

4. Experimental methods

4.1. Modeling

Design and docking of new inhibitors into the active site of HPPK were carried out with program packages CNS and O.^{41,42} The model complex was subject to geometry

optimization using the conjugate gradient method developed by Powell;⁴³ Engh and Huber geometric parameters were used as the basis of the force field.⁴⁴

4.2. Chemistry

4.2.1. General methods—All chemicals were purchased from Sigma-Aldrich except that compound **1** was purchased from TCI America. Starting materials and solvents were used without further purification. Anhydrous reactions were conducted under a positive pressure of dry N₂. Reactions were monitored by TLC, on Baker-flex Silica Gel IB-F (J. T. Baker). All compounds and intermediates were purified by flash chromatography performed on Teledyne ISCO Combiflash Rf system using RediSep Rf columns. Ion exchange chromatography was performed using strata Scx (50 μm particle size, 70 Å pore) resin cartridges. Preparative high pressure liquid chromatography (HPLC) was conducted using a Waters 600E system using a Waters 2487 dual λ absorbance detector and Phenomenex C₁₈ columns (250 mm × 21.2 mm, 5 μm particle size, 110 Å pore) at a flow rate of 10 mL/min. A binary solvent systems consisting of A = 0.1% aqueous TFA and B = 0.1% TFA in acetonitrile was employed with the gradients as indicated. ¹H and ¹³C NMR data were obtained on a Varian 400 MHz spectrometer and are reported in ppm relative to TMS (tetramethylsilane). Mass spectra were measured with Agilent 1100 series LC/Mass Selective Detector, Agilent 1200 LC/MSD-SL system and Thermoquest Surveyor Finnigan LCQ deca. Chemical purity was determined by HPLC analysis with a Zorbax Eclipse plus C18 column (Narrow Bore RR 2.1 mm × 50 mm, 3.5 micron; flow rate of 0.3 mL/min; solvent, methanol:H₂O gradient, 0.1% acetic acid; detection at 260 nm), confirming > 95% purity.

4.2.2. (2-{4-[6-(6-Amino-purin-9-yl)-2,2-dimethyl-tetrahydro-furo[3,4-d][1,3]dioxol-4-ylmethylsulfanyl]-piperidin-1-yl}-ethyl)-carbamic acid tert-butyl ester (7)—To a solution of 9-[2,2-Dimethyl-6-(piperidin-4-ylsulfanylmethyl)-tetrahydro-furo[3,4-d][1,3]dioxol-4-yl]-9H-purin-6-ylamine (**6**) (4.06 g, 10 mmol, 1 eq) and potassium carbonate (2.76g, 20 mmol, 2 eq) in 100 mL acetonitrile, 2-(Boc-amino)ethyl bromide (1.12g, 5 mmol, 0.5eq) was added and then stirred at 50 °C for a few hours before another dose of 2-(Boc-amino)ethyl bromide (1.12g, 5 mmol, 0.5eq) was added. After the reaction was finished, the mixture was evaporated, diluted with EtOAc (100 mL), and washed with saturated aqueous NaHCO₃ (2 × 50 mL) and brine (50 mL). The residue from concentrating the organic layer was purified by silica gel chromatography, eluting with 10% DCM/methanol, to afford 5.43 g (99%) of the title compound as white foam. NMR δH (400 MHz; CD₃OD), 1.39 (3 H, s), 1.42–1.48 (13 H, m), 1.58 (3 H, s), 1.72–1.99 (4 H, m), 2.37 (2 H, t), 2.53–2.58 (1 H, m), 2.75–2.82 (2 H, m), 3.17 (2 H, t), 4.33 (1 H, m), 5.07 (1 H, m), 5.58 (1 H, m), 6.18 (1 H, d), 8.23 (1 H, s), 8.28 (1 H, s); δ¹³C (100 MHz; CD₃OD), 158.32 (1C), 157.46 (1C), 154.03 (1C), 150.25 (1C), 142.05 (1C), 120.65 (1C), 115.33 (1C), 91.88 (1C), 88.87 (1C), 85.25 (1C), 85.07 (1C), 80.05 (1C), 58.75 (1C), 54.18 (2C), 42.29 (1C), 38.41 (1C), 33.56 (1C), 33.44 (1C), 33.28 (1C), 28.75 (3C), 27.35 (1C), 25.48 (1C); MS (ESI) calculated for C₂₅H₃₉N₇O₅ [M+H]⁺ 550.27, found 550.1.

4.2.3. 2-[1-(2-Amino-ethyl)-piperidin-4-ylsulfanylmethyl]-5-(6-amino-purin-9-yl)-tetrahydro-furan-3,4-diol (8)—To a solution of (2-{4-[6-(6-Amino-purin-9-yl)-2,2-dimethyl-tetrahydro-furo[3,4-d][1,3]dioxol-4-ylmethylsulfanyl]-piperidin-1-yl}-ethyl)-carbamic acid tert-butyl ester (**7**) (2.75 g, 5 mmol, 1 eq) in 50 mL DCM, 10 ml TFA was added dropwise at –20 °C and then stirred at room temperature overnight. After the reaction was finished, the solvent was removed under vacuum, and the residue was purified by silica gel chromatography, eluting with 15% DCM/methanol, to afford 1.84 g (90%) of the title compound as white foam. NMR δH (400 MHz; CD₃OD), 1.46–1.54 (4 H, m), 1.84–1.98 (4 H, m), 2.41 (2 H, t), 2.65–2.82 (3 H, m), 2.89–3.02 (2 H, m), 4.20 (1 H, m), 4.37 (1 H, m),

4.80 (1 H, m), 6.0 (1 H, d), 8.21 (1 H, s), 8.31 (1 H, s); $\delta^{13}\text{C}$ (100 MHz; CD_3OD), 157.40 (1C), 153.97 (1C), 150.73 (1C), 141.55 (1C), 120.61 (1C), 90.19 (1C), 86.00 (1C), 74.72 (1C), 73.97 (1C), 59.76 (1C), 54.32 (2C), 42.64 (1C), 38.66 (1C), 33.67 (2C), 33.13 (1C); MS (ESI) calculated for $\text{C}_{17}\text{H}_{27}\text{N}_7\text{O}_3\text{S}$ $[\text{M}+\text{H}]^+$ 410.27, found 410.1.

4.2.4. 2-Amino-7,7-dimethyl-4-oxo-3,4,7,8-tetrahydro-pteridine-6-carboxylic acid (16)—The intermediate **15** was synthesized as described.³⁵ To a solution of **15** (265mg, 1mmol, 1eq) in methanol (5ml) was added a solution of sodium hydroxide (2M, 2mmol, 2eq). After stirring for two hours, the reaction mixture was acidified to pH = 2 with 1M HCl, the product was precipitated, and the precipitate washed once with water and then dried to obtain **16** (213mg, 0.9mmol, 90%). NMR δH (400 MHz; CD_3OD), 1.59 (H, s); $\delta^{13}\text{C}$ (100 MHz; CD_3OD), 166.22 (1C), 161.58 (1C), 157.23 (1C), 156.67 (1C), 142.07 (1C), 101.93 (1C), 36.50 (1C), 29.12 (2C); MS (ESI) calculated for $\text{C}_9\text{H}_{11}\text{N}_5\text{O}_3$ $[\text{M}+\text{H}]^+$ 238.09, found 238.10.

4.2.5. 2-Amino-6-[(2-{4-[5-(6-amino-purin-9-yl)-3,4-dihydroxy-tetrahydro-furan-2-ylmethylsulfanyl]-piperidin-1-yl}-ethylamino)-methyl]-3H-pteridin-4-one (17)—To a solution of **8** (100.0 mg, 0.244 mmol, 1 eq) and potassium carbonate (337.9 mg, 2.44 mmol, 10 eq) in 20 mL dimethylacetamide, **11** (81.7 mg, 0.244 mmol, 1eq) was added and stirred at room temperature for 24 hours. It was evaporated under high vacuum and the residue was dissolved in water methanol mixture and purified by HPLC to give **17** (71.0mg, 0.122 mmol, 50%) as a yellowish powder. NMR δH (400 MHz; CD_3OD), 1.89 (4 H, m), 2.28–2.32 (4 H, m), 3.05–3.3 (3 H, m), 3.53 (2 H, m), 3.63 (2 H, m), 4.22 (1 H, m), 4.35 (1 H, t, J 5.2), 4.41 (2 H, s), 4.74 (1 H, t, J 5.2), 6.05 (1 H, d, J 4.8), 8.37 (1 H, s), 8.47 (1 H, s), 8.76 (1 H, s); $\delta^{13}\text{C}$ (100 MHz; $\text{DMSO}-d_6$), 160.62 (1C), 158.77 (1C), 158.44 (1C), 158.09 (1C), 154.34 (1C), 149.85 (1C), 148.99 (1C), 141.52 (1C), 141.09 (1C), 127.94 (1C), 119.02 (1C), 87.64 (1C), 84.07 (1C), 72.84 (1C), 72.58 (1C), 51.37 (2C), 48.33 (1C), 41.16 (1C), 40.36 (1C), 37.52 (1C), 32.26 (2C), 31.97 (1C); HRMS (ESI-MS) calculated for $\text{C}_{24}\text{H}_{32}\text{N}_{12}\text{O}_4\text{S}$ (MH^+) : 585.2463; found: 585.2460.

4.2.6. 2-Amino-6-[(2-{4-[5-(6-amino-purin-9-yl)-3,4-dihydroxy-tetrahydro-furan-2-ylmethylsulfanyl]-piperidin-1-yl}-ethylamino)-methyl]-7,7-dimethyl-7,8-dihydro-3H pteridin-4-one (18)—To a solution of **8** (100.0 mg, 0.244 mmol, 1 eq) and potassium carbonate (337.9 mg, 2.44 mmol, 10 eq) in 20 mL dimethylacetamide, **13** (89.0 mg, 0.244 mmol, 1eq) was added and stirred at room temperature for 24 hours. It was evaporated under high vacuum and the residue was extracted by methanol. It was evaporated again and the residue was used for direct analysis without further purification. MS (ESI) calculated for $\text{C}_{26}\text{H}_{38}\text{N}_{12}\text{O}_4\text{S}$ $[\text{M}+\text{H}]^+$ 615.29, found 615.10.

4.2.7. 2-Amino-7,7-dimethyl-4-oxo-3,4,7,8-tetrahydro-pteridine-6-carboxylic acid (2-{4-[5-(6-amino-purin-9-yl)-3,4-dihydroxy-tetrahydro-furan-2-ylmethylsulfanyl]-piperidin-1-yl}-ethyl)-amide (19, Method A)³⁶—Compound **8** (12.3 mg, 0.03 mmol, 1.5 eq) was mixed with CuI (0.0388 mg, 0.0002 mmol, 1.0 mol%), AgIO_3 (0.057 mg, 0.0002 mmol, 1.0 mol%), and CaCO_3 (2.2 mg, 0.022 mmol, 1.1 eq) in DMF (0.2 mL). Compound **14** (4.5 mg, 0.020 mmol, 1.0 eq) and T-HYDRO[®] (70 wt% in H_2O , 0.00315 mL, 0.022 mmol, 1.1 eq) were added under an inert atmosphere (N_2) at room temperature. The reaction was allowed to stir overnight at 40 °C. The crude reaction was purified by HPLC (H_2O :Methanol = 2:3) to provide **19** (3.77 mg, 0.006 mmol, 30%) as a pale yellow solid. NMR δH (400 MHz; CD_3OD), 1.58 (6 H, s), 1.76–2.28 (8 H, m), 2.85–3.06 (3 H, m), 3.25 (2H, m) 3.61 (2 H, m), 4.22 (1 H, m), 4.33 (1 H, m), 4.74 (1 H, m), 6.05 (1 H, d, J 4.8), 8.37 (1 H, s), 8.46 (1 H, s); $\delta^{13}\text{C}$ (100 MHz; $\text{DMSO}-d_6$), 164.22 (1C), 157.79 (1C), 155.09 (1C), 155.00 (1C), 148.84 (1C), 143.01 (1C), 141.49 (1C), 118.96 (1C),

117.62 (1C), 114.69 (1C), 100.66 (1C), 87.64 (1C), 84.18 (1C), 72.96 (1C), 72.53 (1C), 55.31 (1C), 53.27 (2C), 51.90 (1C), 37.83 (1C), 33.44 (2C), 31.97 (1C), 29.85 (1C), 27.71 (2C); HRMS (ESI-MS) calculated for C₂₆H₃₆N₁₂O₅S (MH⁺): 629.2725; found: 629.2708.

4.2.8. Compound 19 (Method B)—To a solution of **16** (190 mg, 0.8 mmol, 1eq), *O*-(7-azabenzotriazol-1-yl)-1,1,3,3-tetramethyluronium hexafluorophosphate (HATU) (334.6, 0.88 mmol, 1.1eq), and compound **8** (327.2 mg, 0.8 mmol, 1eq) in anhydrous DMF (100 mL) was added DIPEA (4.18 uL, 2.4 mmol, 3q). After 18 h, the solvent was evaporated under high vacuum, the reaction residue was purified by HPLC (H₂O:Methanol = 2:3) to provide **19** (377 mg, 0.6 mmol, 75%) as a pale yellow solid. NMR and HRMS (ESI-MS) data are found in 4.2.7.

4.3. Fluorometric titration

The dissociation constants of the inhibitors were measured as described³⁷ for the fluorometric measurement of the dissociation constant of Ant-ATP with modifications. Briefly, the inhibitors were dissolved in dimethylsulfoxide. Dimethylsulfoxide concentrations were kept within 1.7% during the titration experiments and control experiments showed that dimethylsulfoxide at these concentrations had no effects on activity (substrate binding and catalysis) of the enzyme. The excitation and emission wavelengths were 420 and 450 nm, respectively, for **17**, but 450 and 480, respectively, for **19**. The excitation and emission slits were 1 and 4 nm, respectively. The titration was performed by adding aliquots of a 500 μM **19** stock solution to an HPPK solution. The initial HPPK concentration and volume were 10 μM and 2 ml, respectively. The *K_d* values were obtained by nonlinear least-squares regression of the data to equation 1 as described³⁷

$$\Delta F_{obs} = \frac{\Delta F_{mol}(K_d + E_t + L_t - \sqrt{(K_d + E_t + L_t)^2 - 4E_t L_t})}{2} \quad (\text{Eq. 1})$$

where Δ*F_{obs}* and Δ*F_{mol}* are observed and molar fluorescence changes caused by binding, *E_t* is the total concentration of HPPK, and *L_t* is the total concentration of the inhibitor. As an example, the fluorometric titration of HPPK with compound **19** is shown in Fig. 6A.

4.4. Enzyme inhibition assay

IC₅₀ measurements were carried out as described¹⁷ except for the concentrations of reaction mixtures, which contained 1 nM *E. coli* HPPK, 2 μM ATP, 1 μM HP, 5 mM MgCl₂, 25 mM DTT, and a trace amount of [α-³²P]-ATP (~1 μCi) in 100 mM Tris, pH 8.3. IC₅₀ values were obtained by fitting the data to a logistic equation by nonlinear least-squares regression of the data to equation 2 as described⁴⁵

$$v = v_{min} + \frac{v_{max} - v_{min}}{1 + \frac{[I]}{IC_{50}}} \quad (\text{Eq. 2})$$

where *v* is the reaction rate, *v_{min}* the minimum reaction rate, *v_{max}* the maximum reaction rate, and [I] the concentration of the inhibitor. The inhibition of HPPK by compound **19** is shown in Fig. 6B.

4.5. Crystallization, X-ray diffraction, structure solution, and refinement

Crystals were grown in sitting drops at 19±1 °C. Crystallization conditions are summarized in Table 1. A Hydra II Plus crystallization robot (Matrix Technologies, Hudson, New Hampshire, USA) and Crystal Screen kits from Hampton Research (Laguna Niguel,

California, USA) were used. X-ray diffraction data were collected at 100K with an MARCCD detector mounted at the synchrotron Beamline 22 at the Advanced Photon Source, Argonne National Laboratory. Data processing was carried out with the HKL2000 program suite.⁴⁶ The structure was solved by Fourier synthesis starting with a homologous structure: PDB entry 1EQM for HPPK•17, 3ILJ for HPPK•18, and 3UDE for HPPK•19. Multiple conformations of amino acid residues, ligands, and solvent molecules were removed from the starting models. Structure solution and refinement were done with PHENIX.⁴⁷ All graphics work, including model building and rebuilding, was performed with COOT.⁴⁸ The structures were verified with annealed omit maps and the geometry was assessed using PROCHECK⁴⁹ and WHAT IF.⁵⁰ The statistics of X-ray diffraction data and structures are summarized in Table 2. Illustrations were prepared with PyMOL.⁵¹

Supplementary Material

Refer to Web version on PubMed Central for supplementary material.

Acknowledgments

This research was supported by NIH grant GM51901 (H.Y.), NIAID Trans NIH/FDA Intramural Biodefense Program Y3-RC-8007-01 (X.J.), and the Intramural Research Program of the NIH, National Cancer Institute, Center for Cancer Research. Mass spectrometry experiments were conducted on an Agilent 1100 series LC/Mass Selective Detector maintained by the Biophysics Resource in the Structural Biophysics Laboratory, an Agilent 1200 LC/MSD-SL system in the Chemical Biology Laboratory, and a Thermoquest Surveyor Finnigan LCQ deca maintained by the Comparative Carcinogenesis Laboratory of National Cancer Institute at Frederick. X-ray diffraction data were collected at the Southeast Regional Collaborative Access Team (SER-CAT) 22-ID and 22-BM beamlines at the Advanced Photon Source (APS), Argonne National Laboratory (ANL).

Abbreviations

AMPCPP	α,β -methyleneadenosine 5'-triphosphate
HP	6-hydroxymethyl-7,8-dihydropterin
HP-1	6-hydroxymethyl-7,7-dimethyl-7,8-dihydropterin
HP-3	6-hydroxymethyl-7-methyl-7-phenethyl-7,8-dihydropterin
HP₂A	P^1 -(6-hydroxymethylpterin)- P^2 -(5'-adenosyl)diphosphate
HP₃A	P^1 -(6-hydroxymethylpterin)- P^3 -(5'-adenosyl)triphosphate
HP₄A	P^1 -(6-hydroxymethylpterin)- P^4 -(5'-adenosyl)tetraphosphate
HPPK	6-hydroxymethyl-7,8-dihydropterin pyrophosphokinase
HPPP	6-hydroxymethyl-7,8-dihydropterin pyrophosphate
PDB	Protein Data Bank

References

1. Blakley, RL.; Benkovic, SJ. Foliates and Pterins. Blakley, RL.; Benkovic, SJ., editors. John Wiley & Sons, Inc; New York: 1984.
2. Hitchings GH, Burchall JJ. Adv Enzymol Relat Areas Mol Biol. 1965; 27:417–468. [PubMed: 4387360]
3. Cohen ML. Science. 1992; 257:1050–1055. [PubMed: 1509255]
4. Neu HC. Science. 1992; 257:1064–1073. [PubMed: 1509257]
5. Kunin CM. Ann Intern Med. 1993; 118:557–561. [PubMed: 8442626]
6. Levy SB. Adv Exp Med Biol. 1995; 390:1–13. [PubMed: 8718598]

7. Murray BE. *Adv Intern Med*. 1997; 42:339–367. [PubMed: 9048124]
8. Bermingham A, Derrick JP. *Bioessays*. 2002; 24:637–648. [PubMed: 12111724]
9. Walsh C. *Nat Rev Microbiol*. 2003; 1:65–70. [PubMed: 15040181]
10. Hughes, DTD. *Sulphonamides Antibiotic and Chemotherapy*. 7. Churchill Livingstone; New York: 1997.
11. Hughes, DTD. *Antibiotics and Chemotherapy*; O'Grady, F.; Lambert, HP.; Finch, RG.; Greenwood, D., editors. Churchill Livingstone; New York: 1997. p. 346-356.
12. Zinner, SH.; Mayer, KH. *Principles and Practice of Infectious Diseases*; Mandell, GL.; Bennett, JE.; Dolin, R., editors. Churchill Livingstone; Philadelphia: 2005. p. 440-451.
13. Wood, HCS. *Chemistry and Biology of Pteridines*; Pfeleiderer, W., editor. Walter de Gruyter; Berlin-New York: 1975.
14. Al-Hassan SS, Cameron RJ, Curran AWC, Lyall WJS, Nicholson SH, Robinson DR, Stuart A, Suckling CJ, Stirling I, Wood HCS. *J Chem Soc, Perkin Trans*. 1985; 1:1645–1659.
15. Hennig M, Dale GE, D'Arcy A, Danel F, Fischer S, Gray CP, Jolidon S, Muller F, Page MG, Pattison P, Oefner C. *J Mol Biol*. 1999; 287:211–219. [PubMed: 10080886]
16. Stammers DK, Achari A, Somers DO, Bryant PK, Rosemond J, Scott DL, Champness JN. *FEBS Lett*. 1999; 456:49–53. [PubMed: 10452528]
17. Shi G, Blaszczyk J, Ji X, Yan H. *J Med Chem*. 2001; 44:1364–1371. [PubMed: 11311059]
18. Shiota, T. *Chemistry and Biochemistry of Folates*; Blakley, RT.; Benkovic, SJ., editors. John Wiley & Sons; New York: 1984. p. 121-134.
19. Shi G, Gong Y, Savchenko A, Zeikus JG, Xiao B, Ji X, Yan H. *Biochim Biophys Acta*. 2000; 1478:289–299. [PubMed: 10825540]
20. Bermingham A, Bottomley JR, Primrose WU, Derrick JP. *J Biol Chem*. 2000; 275:17962–17967. [PubMed: 10751386]
21. Li Y, Gong Y, Shi G, Blaszczyk J, Ji X, Yan H. *Biochemistry*. 2002; 41:8777–8783. [PubMed: 12093297]
22. Xiao B, Shi G, Chen X, Yan H, Ji X. *Structure*. 1999; 7:489–496. [PubMed: 10378268]
23. Neuhard, J.; Nygaard, P. *Escherichia coli and Salmonella typhimurium: Cellular and Molecular Biology*; Neidhardt, FC.; Ingraham, JL.; Low, KB.; Magasanik, B.; Schaechter, M.; Umberger, HE., editors. ASM Press; Washington, D. C: 1987. p. 445-473.
24. Derrick, JP. *Folic Acid and Folates*; Litwack, G., editor. Academic Press; Oxford, UK: 2008. p. 411-433.
25. Yan H, Ji X. *Protein Pept Lett*. 2011; 18:328–335. [PubMed: 21222642]
26. Kompis IM, Islam K, Then RL. *Chem Rev*. 2005; 105:593–620. [PubMed: 15700958]
27. Blaszczyk J, Shi G, Yan H, Ji X. *Structure*. 2000; 8:1049–1058. [PubMed: 11080626]
28. Blaszczyk J, Li Y, Shi G, Yan H, Ji X. *Biochemistry*. 2003; 42:1573–1580. [PubMed: 12578370]
29. Broom AD. *J Med Chem*. 1989; 32:2–7. [PubMed: 2642553]
30. Radzicka A, Wolfenden R. *Methods Enzymol*. 1995; 249:284–312. [PubMed: 7791615]
31. Sakami W. *Biochemical Preparations*. 1961; 8:5–8.
32. Plettenburg, O.; Hofmeister, A.; Goerlitzer, J.; LÖHn, M. WO Patent. WO/2008/077,552. 2008.
33. Isakovic L, Saavedra OM, Llewellyn DB, Claridge S, Zhan L, Bernstein N, Vaisburg A, Elowe N, Petschner AJ, Rahil J. *Bioorg Med Chem Lett*. 2009; 19:2742–2746. [PubMed: 19364644]
34. Stuart, A. US Patent. 4,036,961. 1977.
35. Shi G, Ji X. *Tetrahedron Lett*. 2011; 52:6174–6176. [PubMed: 22125346]
36. Yoo WJ, Li CJ. *J Am Chem Soc*. 2006; 128:13064–13065. [PubMed: 17017781]
37. Li Y, Wu Y, Blaszczyk J, Ji X, Yan H. *Biochemistry*. 2003; 42:1581–1588. [PubMed: 12578371]
38. Xiao B, Shi G, Gao J, Blaszczyk J, Liu Q, Ji X, Yan H. *J Biol Chem*. 2001; 276:40274–40281. [PubMed: 11546767]
39. Blaszczyk J, Shi G, Li Y, Yan H, Ji X. *Structure (Camb)*. 2004; 12:467–475. [PubMed: 15016362]
40. Li G, Felczak K, Shi G, Yan H. *Biochemistry*. 2006; 45:12573–12581. [PubMed: 17029412]

41. Brünger AT, Adams PD, Clore GM, DeLano WL, Gros P, Grosse-Kunstleve RW, Jiang JS, Kuszewski J, Nilges M, Pannu NS, Read RJ, Rice LM, Simonson T, Warren GL. *Acta Crystallogr D*. 1998; 54:905–921. [PubMed: 9757107]
42. Jones TA, Kjeldgaard M. *Methods Enzymol*. 1997; 277:173–208. [PubMed: 18488310]
43. Powell MJD. *Math Prog*. 1977; 12:241–254.
44. Engh RA, Huber R. *Acta Crystallogr A*. 1991; 47:392–400.
45. Graeser, D.; Neubig, RR. *Signal transduction*; Milligan, G., editor. IRL Press; Oxford: 1992. p. 1-30.
46. Otwinowski Z, Minor W. *Methods Enzymol*. 1997; 276:307–326.
47. Adams PD, Grosse-Kunstleve RW, Hung LW, Ioerger TR, McCoy AJ, Moriarty NW, Read RJ, Sacchettini JC, Sauter NK, Terwilliger TC. *Acta Crystallogr D*. 2002; 58:1948–54. [PubMed: 12393927]
48. Emsley P, Cowtan K. *Acta Crystallogr D*. 2004; 60:2126–32. [PubMed: 15572765]
49. Laskowski RA, MacArthur MW, Moss DS, Thornton JM. *J Appl Crystallogr*. 1993; 26:283–291.
50. Vriend G. *J Mol Graph*. 1990; 8:52–56. 29. [PubMed: 2268628]
51. DeLano, WL. *Delano Scientific*. San Carlos, CA: 2002.
52. Lovell SC, Davis IW, Arendall WB 3rd, de Bakker PI, Word JM, Prisant MG, Richardson JS, Richardson DC. *Proteins: Struct Funct Genet*. 2003; 50:437–450. [PubMed: 12557186]

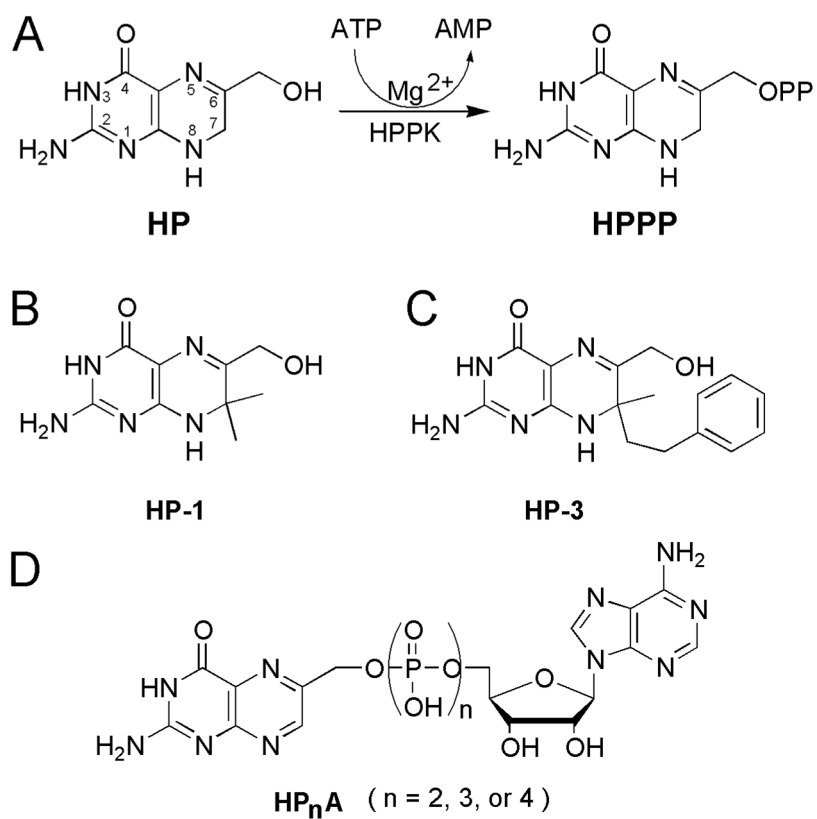


Figure 1. Reaction and molecular structures of previous HPPK inhibitors. (A) Reaction catalyzed by HPPK and chemical structures of substrate HP and product HPPP. (B–D) HPPK inhibitors HP-1,^{13,15} HP-3,¹⁶ and HP_nA (n=2,3, or 4).¹⁷

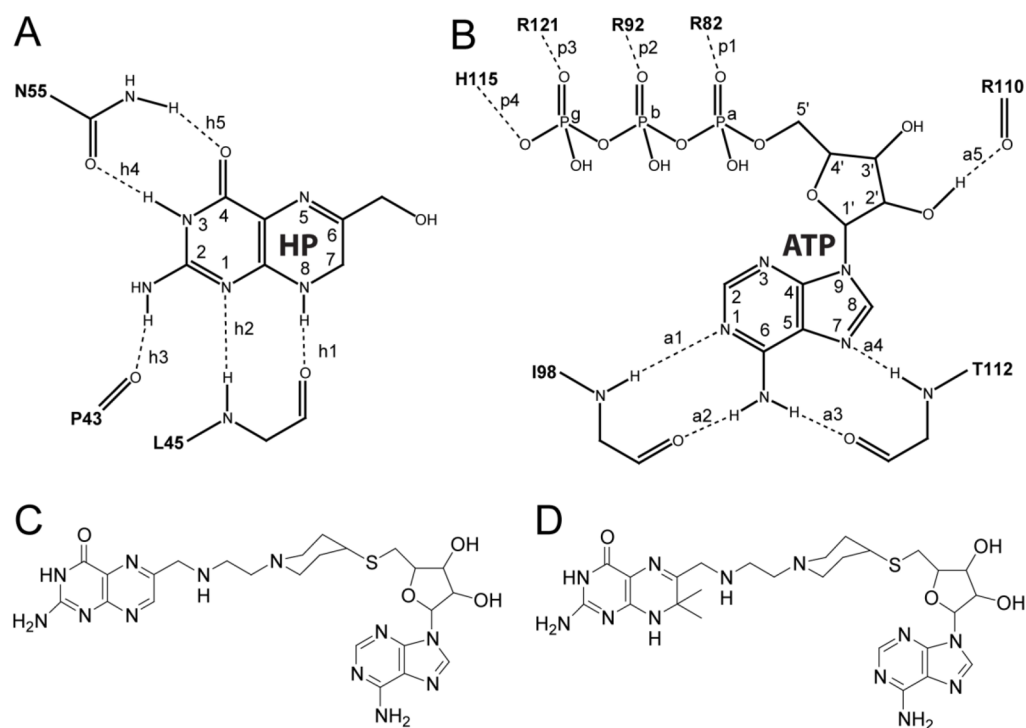


Figure 2. Protein-ligand interaction and inhibitor design. (A, B) Optimized hydrogen bond interactions between HPPK and HP/ATP on the basis of the HPPK•MgAMPCPP•HP (PDB entry 1Q0N), HPPK•MgATP•HP-3 (1DY3), and HPPK•MgAMPCPP•HP-analogs (3IP0) structures. (C, D) New design of bisubstrate analog inhibitors of HPPK.

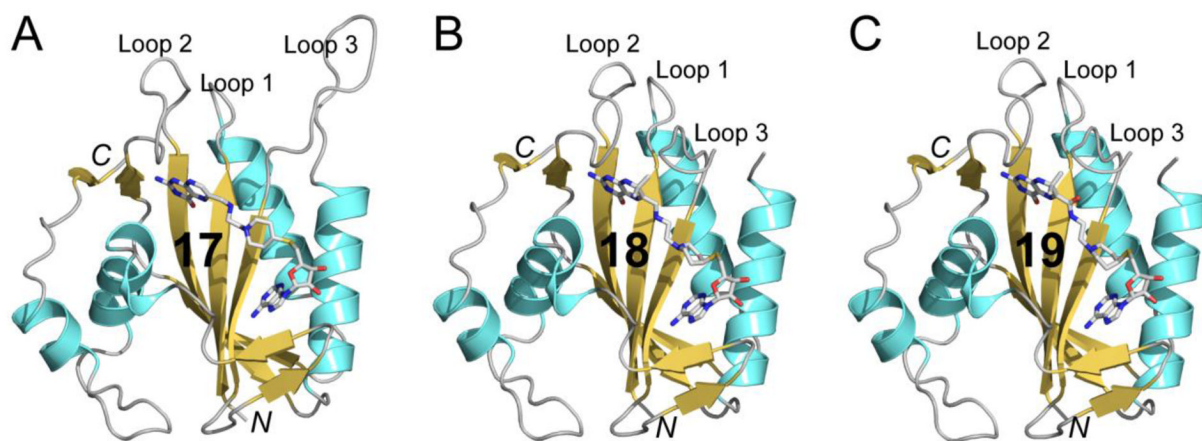


Figure 3. Schematic illustration of crystal structures. (A) The HPPK•17 complex. (B) The HPPK•18 complex. (C) The HPPK•19 complex. Polypeptide chains are shown as a ribbon diagrams with helices (spirals) in cyan, strands (arrows) in orange, and loops (tubes) in grey. Ligands are shown as sticks in atomic color scheme (C in grey, N in blue, O in red, P in orange, and S in orange).

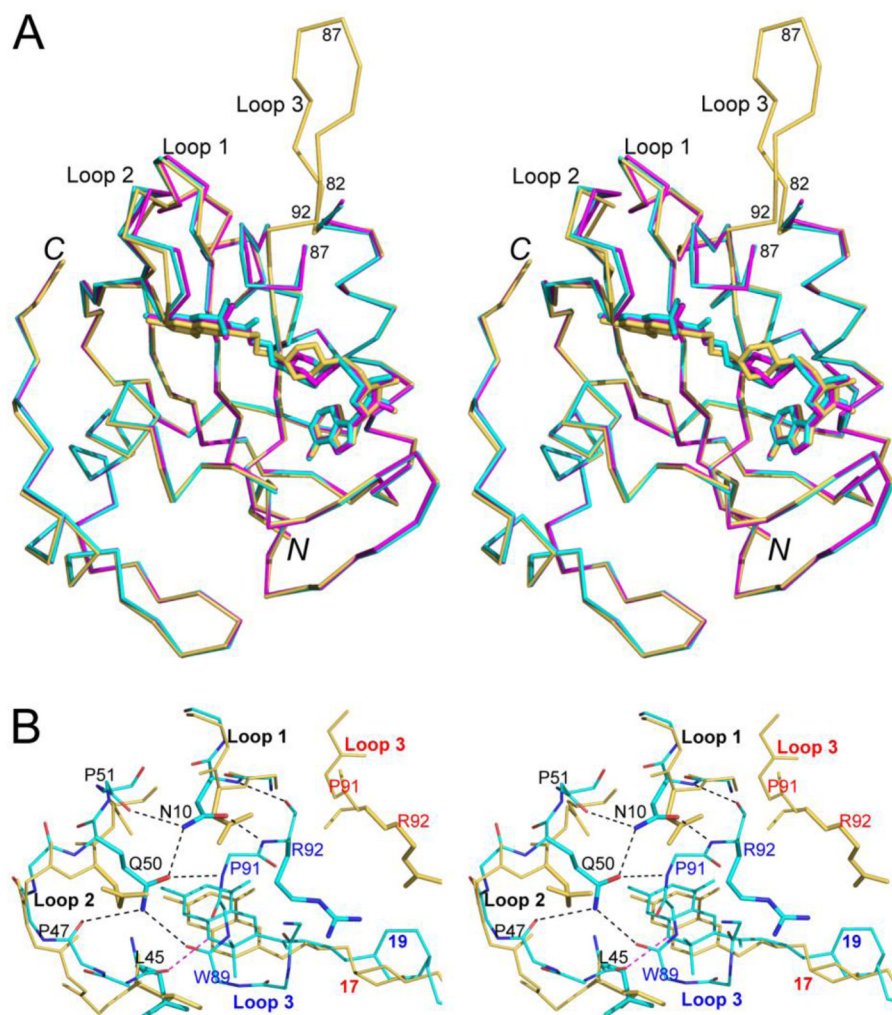


Figure 4. Structural comparison in stereo. (A) The HPPK•17 (in orange), HPPK•18 (in magenta), and HPPK•19 (in cyan) structures are superimposed. Proteins are shown as Ca traces and ligands as sticks. (B) Coupled loops in HPPK•19 (in cyan, those in HPPK•18 are not shown for clarity) versus uncoupled loops in HPPK•17 (in orange). Hydrogen bonds are indicated by dashed lines in black, but the N8^{Pterin}...O^{L45} interaction is highlighted in magenta. Labels are color coded: blue for HPPK•19, red for HPPK•17, and black for the common features in both. For clarity, most side chains that are not involved in loop coupling are not shown.

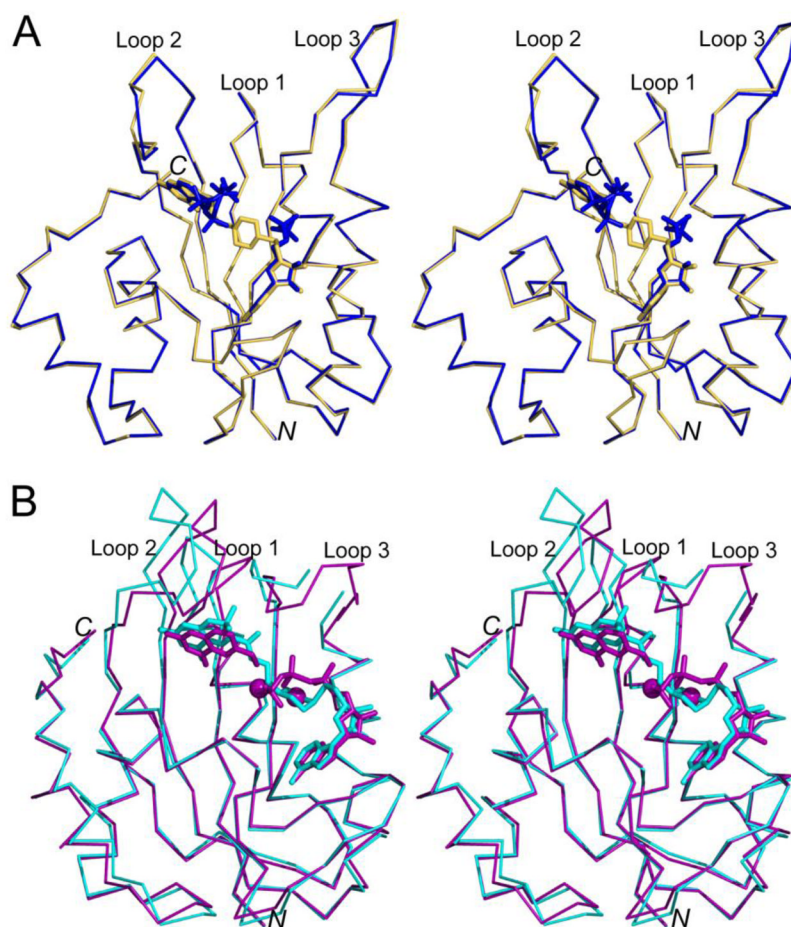


Figure 5. Comparison of new with related structures in stereo. (A) The HPPK•17 (in orange, this work) and HPPK•AMP•HPPP (in blue, PDB entry 1RAO) structures are superimposed. (B) The HPPK•19 (in cyan, this work) and HPPK•MgAMPCPP•HP (in purple, PDB entry 1Q0N) structures are superimposed. Proteins are shown as Ca traces and ligands as sticks.

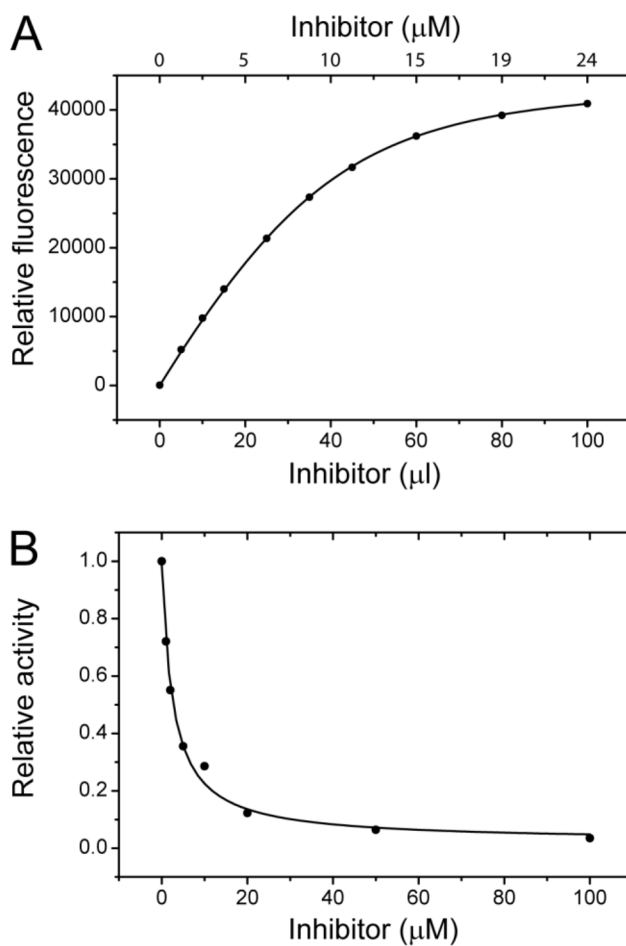
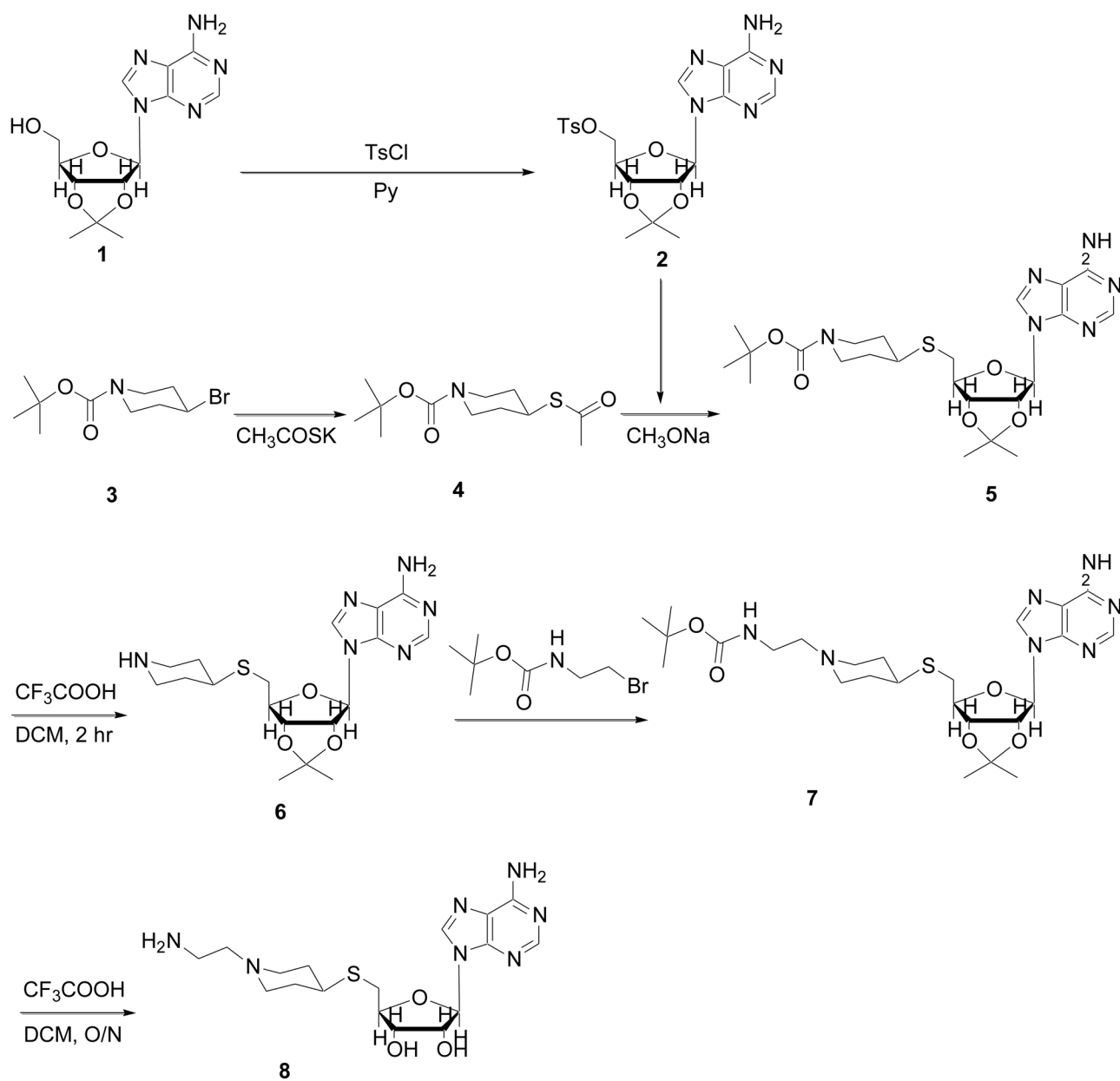
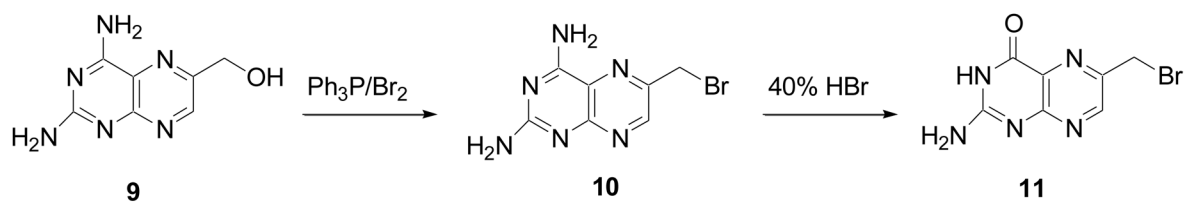


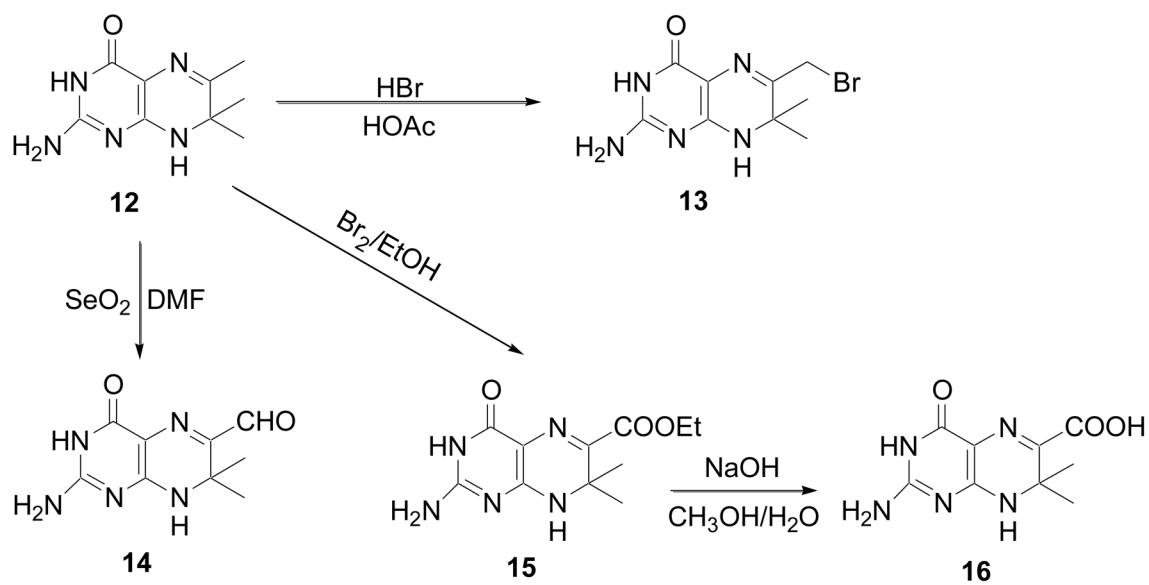
Figure 6. K_d and IC_{50} measurements. (A) Fluorometric titration of HPPK with compound **19**. (B) Inhibition of HPPK by **19**.



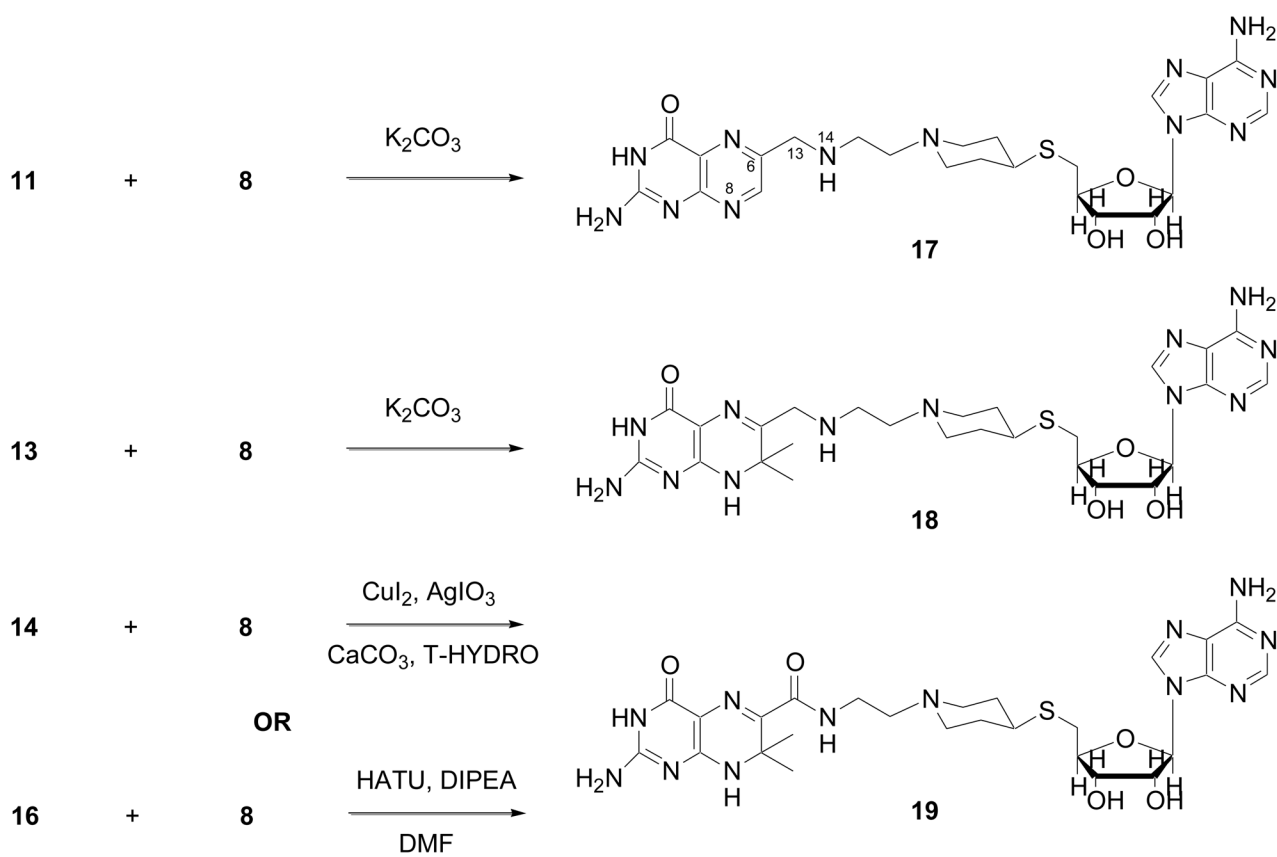
Scheme 1.



Scheme 2.



Scheme 3.



Scheme 4.

Table 1

Crystallization conditions

	HPPK•17	HPPK•18	HPPK•19
PDB Entry Code	3UD5	3UDE	3UDV
Protein Solution			
HPPK (mg/mL)	10	10	10
Compound 17	Saturated		
Compound 18		Saturated	
Compound 19			Saturated
Tris-HCl [mM (pH)]	20 (8.0)	20 (8.0)	20 (8.0)
Reservoir Solution			
PEG 3350 [% (w/v)]	25	25	20
CH ₃ -COONH ₄ (mM)		200	200
Bis-Tris [mM (pH)]	100 (6.5)	100 (8.5)	
HEPES [mM (pH)]			100 (7.5)
Crystals			
Appear (days)	7	7	14
Reach final size (days)	14	14	21
Shape	Thin plate	Thin plate	Thin plate
Dimension (mm)	0.15 × 0.10 × 0.005	0.10 × 0.05 × 0.005	0.15 × 0.10 × 0.005

Table 2

Crystal data, X-ray diffraction, and structures

	HPPK•17	HPPK•18	HPPK•19
PDB Entry Code	3UD5	3UDE	3UDV
Crystal			
Space group	<i>C</i> 2	<i>P</i> 21212	<i>P</i> 21212
Unit cell parameters: <i>a</i> (Å)	79.98	52.91	53.00
<i>b</i> (Å)	52.77	70.98	70.64
<i>c</i> (Å)	36.69	36.38	36.25
β (°)	102.70	90	90
Matthews coefficient (Å ³ /Da)	2.1	1.9	1.9
Data			
	Overall (last shell)	Overall (last shell)	Overall (last shell)
Resolution (Å)	30.00–1.90 (1.97–1.90)	30.00–1.82 (1.89–1.82)	30.00–1.79 (1.85–1.79)
Unique reflections	10236 (717)	11525 (650)	11716 (658)
Redundancy	6.5 (5.3)	6.1 (2.5)	6.0 (2.8)
Completeness (%)	87.0 (61.7)	89.7 (51.9)	87.6 (50.4)
R_{merge}^a	0.089 (0.320)	0.084 (0.561)	0.074 (0.322)
I/σ	16.2 (3.8)	16.7 (1.3)	19.1 (2.3)
Refinement			
	Overall (last shell)	Overall (last shell)	Overall (last shell)
Resolution (Å)	29.84–2.00 (2.13–2.00)	29.48–1.88 (1.98–1.88)	29.92–1.88 (1.98–1.88)
Unique reflections	9252 (1203)	10902 (1180)	10754 (1150)
Completeness (%)	90.7 (72.0)	93.5 (73.0)	92.8 (72.0)
Data in the test set	824 (107)	949 (104)	920 (98)
R-work	0.158 (0.164)	0.178 (0.243)	0.210 (0.253)
R-free	0.205 (0.262)	0.237 (0.309)	0.275 (0.288)
Structure			
Protein non-H atoms/B (Å ²)	1448/30.0	1389/28.1	1399/26.4
Ligand atoms/B (Å ²)	49/44.4	47/31.3	48/40.7
Water oxygen atoms/B (Å ²)	106/38.3	88/36.1	91/32.8
Rmsd			
Bond lengths (Å)	0.012	0.012	0.013
Bond angles (°)	1.302	1.382	1.376
Coordinate error (Å)	0.54	0.50	0.48
Ramachandran plot ^b			
Favored regions (%)	98.7	97.3	97.3
Disallowed regions (%)	0.0	0.0	0.0

^a $R_{\text{merge}} = \sum(|I - \langle I \rangle|) / \sum(I)$, where *I* is the observed intensity.

^bObtained using Ramachandran data by Lovell and coworkers.⁵²